IJMMS, *Vol. 13, No. 1, (January-June 2017):215-242*

ISSN: 0973-3329

INFLUENCE OF MAGNETIC FIELD ON NATURAL CONVECTIVE CHEMICALLY REACTING JEFFERY FLUID FLOW PAST AN INFINITE VERTICALLY INCLINED PLATE EMBEDDED IN POROUS MEDIUM: A FINITE DIFFERENCE TECHNIQUE

M.V. Ramana Murthy* and Y. Sunita Rani**

Abstract

The study of this is article is the combined influence of heat transfer and mass transfer on an unsteady magneto hydrodynamic free convective Jeffrey fluid flow over an infinite vertical plate embedded in a saturated porous medium in presence of thermal radiation, hall current and angle of inclination. Suitable dimensionless variables are employed to the non-linear coupled governing equations and the numerical solutions are obtained for velocity, temperature and concentration profiles using the finite difference technique. The numerical results for various controlling parameters are shown graphically and discussed in details. Expressions for skin-friction, Nusselt and Sherwood numbers are also evaluated and presented in tabular forms. A comparative study of the present numerical results with the analytical results from the earlier works provides an excellent agreement.

Keywords: *Heat transfer; Mass transfer; Jeffrey fluid; MHD; Finite difference method.*

Nomenclature:

List of variables:

T	*Temperature of fluid near the plate (K)*
T_w	*Temperature of the fluid far away of the fluid from the plate (K)*
T_∞	*Temperature of the fluid at infinity (K)*

* Department of Mathematics& Computer Science, University College for Sciences, Osmania University, Hyderabad-500007, Telangana State, India

** Research Scholar, Department of Mathematics, Rayalaseema University, Kurnool-518002, Andhra Pradesh, India. *Email: ysunitarani@gmail.com*

t	*Time in x, y coordinate system (second)*
u	*Velocity component in x-direction (m/s)*
U	*Dimensionless velocity component in x- direction (m/s)*
w	*Velocity component in z-direction (m/s)*
W	*Dimensionless velocity component in z- direction (m/s)*
x, y	*Co-ordinate system (m)*
u_o	*Reference velocity (m/s)*
v_o	*Suction velocity (m/s)*
g	*Acceleration of gravity, 9.81 (m/s^2)*
B_o	*Magnetic field component along y- axis (Tesla)*
C_p	*Specific heat at constant pressure (J-K/Kg)*
Gr	*Grashof number for heat transfer*
Gc	*Grashof number for mass transfer*
M	*Magnetic field parameter*
Nu	*Rate of heat transfer coefficient (or) Nusselt number*
Sh	*Rate of mass transfer coefficient (or) Sherwood number*
m	*Hall parameter*
Pr	*Prandtl number*
Re	*Reynold's number*
C_x	*Skin-friction coefficient due to primary velocity (N/m^2)*
C_z	*Skin-friction coefficient due to secondary velocity (N/m^2)*
O	*Origin*
$v_0 > 0$	*Suction*
$v_0 < 0$	*Injection*
a_0	*Half of non-dimensional transpiration parameter*
$\bar{K}$	*Homogeneous Chemical reaction of first order*
Sc	*Schmidt number*
D	*Chemical molecular diffusivity ($m^2 s^{-1}$)*
C_∞	*Concentration of fluid in free stream (mol m^{-3})*
C	*Concentration of fluid within boundary layer (mol m^{-3})*
C_w	*Characteristic concentration of fluid (mol m^{-3})*

K_r *Dimensional chemical reaction parameter*

h *Length scale of similarity parameter (m)*

v *Velocity component in y-direction ($m\ s^{-1}$)*

k_r *Chemical reaction parameter*

q_r *Radiative heat flux*

k^* *Mean absorption coefficient*

S *Heat Source parameter*

Q *Non dimensional Heat Source parameter*

Greek Symbols:

β *Coefficient of volume expansion for heat transfer (K^{-1})*

β^* *Coefficient of volume expansion for mass transfer ($m^3\ Kg^{-1}$)*

κ *Thermal conductivity of the fluid (W/mK)*

σ *Electrical conductivity of the fluid ($\Omega^{-1}\ m^{-1}$)*

ν *Kinematic viscosity ($m^2\ s^{-1}$)*

θ *Non-dimensional temperature (K)*

ρ *Density of the fluid (kg/m^{-3})*

α *Angle of inclination (degrees)*

λ *Jeffrey fluid parameter*

η *Dimensionless coordinate (m)*

μ_e *Magnetic permeability of the medium (m^2)*

ϕ *Non-dimensional concentration of fluid ($mol\ m^{-3}$)*

σ_o *Stefan-Boltzmann constant*

Superscript:

$'$ *Dimensionless properties*

Subscripts:

p *Plate*

w *Conditions on the wall*

∞ *Free stream conditions*

1. INTRODUCTION

Non-Newtonian transport phenomena arise in many branches of process mechanical, chemical and materials engineering. Such fluids exhibit shear-stress-strain relationships which diverge significantly from the classical Newtonian (Navier-Stokes) model. Most non-Newtonian models involve some form of modification to the momentum conservation equations. These include power-law fluids [1], viscoelastic fluid model [2], Walters-B short memory models [3], Oldroyd-B models [4], differential Reiner-Rivlin models [5] and [6], Bingham plastics [7], tangent hyperbolic models [8], Eyring-Powell models [9], nano non-Newtonian fluid models [10] and Maxwell models [11]. Among the several non-Newtonian models proposed, Jeffrey's fluid model is significant because Newtonian fluid model can be deduced from this as a special case by taking $\lambda_1 = 0$. Further, it is speculated that the physiological fluids such as blood exhibit Newtonian and non-Newtonian behaviours during circulation in a living body. As with a number of rheological models developed, the Jeffrey's model has proved quite successful. This simple, yet elegant rheological model was introduced originally to simulate earth crustal flow problems [12]. This model [13] constitutes a viscoelastic fluid model which exhibits shear thinning characteristics, yield stress and high shear viscosity. The Jeffrey's fluid model degenerates to a Newtonian fluid at a very high wall shear stress i.e. when the wall stress is much greater than yield stress. This fluid model also approximates reasonably well the rheological behaviour of other liquids including physiological suspensions, foams, geological materials, cosmetics, and syrups.

Mass transfer refers to the transfer or movement of mass from one location/component to another. In a variety of engineering processes, mass transfer is of common occurrence. Particularly, in the field of chemical engineering, study of mass transfer is of vital importance, more specifically in the branches of heat transfer engineering, separation process engineering and reaction engineering. The rate at which mass transfer takes place depends on flow pattern and diffusivity. In various studies, mass transfer coefficients are usually considered as dimensionless parameters, e.g. Schmidt number, Sherwood number, and Reynolds number. It is interesting to note that the approximate differential equations used in the study of variety of physical problems of fluid dynamics (at low Reynolds number) that represent the conservation of momentum, mass and energy are somewhat analogous [14] and [15]. An analytical solution to a problem of estimating particle-to-fluid heat and mass transfer rates in multiparticle systems at low Reynolds numbers was put forward by Pfeffer and Happel [16]. A problem of heat and mass transfer during MHD flow of a viscous fluid in a vertical plate was discussed by

Singh et al. [17], by considering the fluid to be incompressible and electrically conducting. The vertical plate was assumed to be porous and to be embedded in a porous medium, whose permeability is time-dependent. Under these assumptions, the effect of oscillatory suction velocity normal to the plate was studied for a situation, where the action of the applied magnetic field is uniform and permeability of the medium fluctuates with time. The study shows that the amplitude, phase and the skin friction coefficient due to heating the plate are similar to the case of cooling. However, the phase lag in the case of heating the plate is more than that for cooling. Some more interesting studies related to the effects of heat and mass transfer on MHD channel flows were investigated recently by Gul et al. [18] and [19], Zin et al. [20] and Khalid et al. [21]. These studies bear the promise of important applications in different industrial problems. Heat transfer during MHD mixed convection flows of ferrofluids in a vertical channel was investigated in [18], while [19] deals with an important problem of the effects of energy transfer on mixed convection channel flows of nanofluids. The channel was considered to be submerged in a saturated porous medium. The fluid considered was supposed to contain nano-particles of different shapes. On the basis of these two studies, the authors made an important observation that for both ferrofluids and nanofluids, the fluid velocity and temperature are highly influenced by fluid viscosity and thermal conductivity. It was remarked on the basis of the study [19] that in comparison with water, ethylene glycol is considered as a better base fluid for convection owing to the fact that its viscosity and thermal conductivity are higher than those of water. Zin et al. [20] and Khalid et al. [21] deal with two different problems of MHD free convection flows past vertical plates embedded in porous media. In [20], the fluid considered is a Jeffrey fluid containing nano-particles of silver. They observed that a rise in volume fraction is accompanied by an increase in fluid velocity and a rise in fluid temperature. Heat transfer during flow of a ferrofluid that contains nano-particles of cylindrical shape was investigated in [21] for the case of ramp-type heating of a vertical plate on which the fluid flow occurs. This study may have some impact on drug delivery to breast cancer cells. Chamkha et al. [22] investigated the effects of chemical reaction, thermal radiation and heat generation or absorption on unsteady free convective heat and mass transfer along an infinite vertical porous plate in the presence of a transverse magnetic field and Hall current using a fourth-order Runge-Kutta scheme along with the shooting method.

The purpose of this paper is to examine numerically the effects of thermal radiation, chemical reaction and hall current on viscous, electrically conducting and incompressible Jeffrey fluid towards an infinite vertical plate filled with porous material. Numerical solutions obtained by applying finite difference

method for primary and secondary velocities, temperature, concentration profiles, skin-friction, rate of heat and mass transfer coefficients are obtained and the effects of governing parameters are discussed with the aid of line graphs.

2. MATHEMATICAL ANALYSIS

Consider magnetohydrodynamic free convective flow of a viscous, incompressible and electrically conducting Jeffrey fluid towards an infinite vertically inclined plate embedded in porous medium subjected to time-dependent suction velocity. The physical coordinate of the problem is as shown in the Figure 1. The flow is assumed along $x-$axis which is taken along the plate in the upward direction and the $y-$axis perpendicular to it. Let us assume that all physical quantities will be independent of $x-$direction. Therefore, all the physical variables become functions of y and t only. In $y-$direction, the uniform strong magnetic field B_o is assumed. The transverse applied magnetic field and magnetic Reynolds number are assumed to be very small, so that the induced magnetic field is negligible. The homogeneous chemical reaction of first order with rate constant $\overline{K}$ between the diffusing species and the fluid is assumed. The wall is maintained at constant temperature T_w and concentration C_w higher than the ambient temperature T_∞ and concentration C_∞ respectively. In energy equation, the viscous dissipation and the joule heating effects are negligible. Let us assume that electric field is neglected. All the fluid properties except the density in the buoyancy force term are constant and the plate is electrically non-conducting. The Cauchy stress tensor, $\overline{S}$, of a Jeffrey's non-Newtonian fluid [23] takes the form as follows:

$$S = \frac{\mu}{1+\lambda}\left(\dot{\gamma} + \lambda_1 \ddot{\gamma}\right) \tag{1}$$

where, μ is the dynamic viscosity, λ_1 is the ratio of relaxation to retardation times, dot above a quantity denotes the material time derivative and γ is the shear rate. The Jeffrey's model provides an elegant formulation for simulating retardation and relaxation effects arising in non-Newtonian polymer flows. The shear rate and gradient of shear rate are further defined in terms of velocity vector, $\overline{V}$, as follows:

where, $$\dot{\gamma} = \nabla \overline{V} + \left(\nabla \overline{V}\right)^T \tag{2}$$

and $$\ddot{\gamma} = \frac{d}{dt}\left(\dot{\gamma}\right) + \left(\overline{V}.\nabla\right)\dot{\gamma} \tag{3}$$

Under these assumptions with the usual Boussinesq's approximation, the governing boundary-layer equations ([24]) that are based on the balance laws of mass, linear momentum, energy and concentration species for this investigation can be written as:

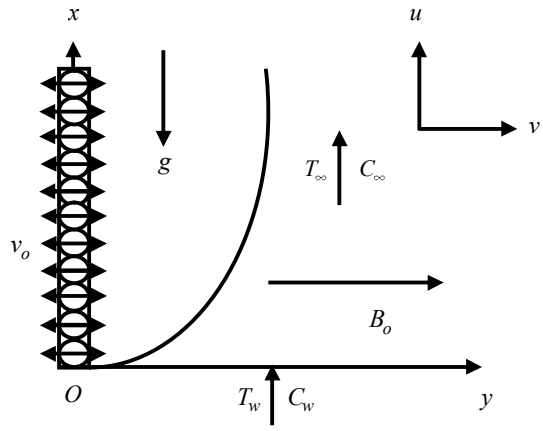

Figure 1. Physical configuration and coordinates system

Equation of Continuity:

$$\frac{\partial v}{\partial y}=0 \tag{4}$$

Momentum Equations:

$$\frac{\partial u}{\partial t}+v\frac{\partial u}{\partial y}=\left(\frac{\nu}{1+\lambda}\right)\frac{\partial^2 u}{\partial y^2}-\frac{1}{\left(1+m^2\right)}\left[\frac{\sigma\mu_e^2 {B_0}^2}{\rho}\right]u-\frac{m\mu_e^2\sigma {B_0}^2}{\rho\left(1+m^2\right)}w$$

$$+g\beta\left(T-T_\infty\right)\left(\cos\alpha\right)+g\beta^*\left(C-C_\infty\right)\left(\cos\alpha\right) \tag{5}$$

$$\frac{\partial w}{\partial t}+v\frac{\partial w}{\partial y}=\nu\frac{\partial^2 w}{\partial y^2}+\frac{\sigma {B_0}^2\mu_e^2}{\rho\left(1+m^2\right)}\left(mu-w\right) \tag{6}$$

Energy equation:

$$\frac{\partial T}{\partial t}+v\frac{\partial T}{\partial y}=\frac{\kappa}{\rho C_p}\frac{\partial^2 T}{\partial y^2}-\frac{1}{\rho C_p}\left(\frac{\partial q_r}{\partial y}\right)+\frac{Q}{\rho C_p}\left(T-T_\infty\right) \tag{7}$$

Species diffusion equation:

$$\frac{\partial C}{\partial t}+v\frac{\partial C}{\partial y}=D\frac{\partial^2 C}{\partial y^2}-K_r\left(C-C_\infty\right) \tag{8}$$

The corresponding boundary conditions are given by

$$\left\{\begin{array}{l} t \le 0 : \left\{u = 0,\ \ w = 0,\ \ T = T_\infty,\ \ C = C_\infty \quad \textit{for all } y\right\} \\ t > 0 : \begin{cases} u = 0,\ \ w = 0,\ \ T = T_w,\ \ C = C_w & \textit{at } y = 0 \\ u \to 0,\ w \to 0, T \to T_\infty,\ C \to C_\infty & \textit{at } y \to 0 \end{cases} \end{array}\right\} \tag{9}$$

The radiative heat flux term is simplified by using the Rosseland approximation (see Sparrow and Cess [25]) as

$$q_r = -\frac{4\sigma_o}{3k^*}\left(\frac{\partial T^4}{\partial y}\right) \tag{10}$$

The obtained Taylor series expansion for T^4 neglecting the higher order terms:

$$T^4 = 4T_\infty^3 T - 3T_\infty^4 \tag{11}$$

Using equations (10) and (11) in energy equation (7), we obtain

$$\frac{\partial T}{\partial t} + v\frac{\partial T}{\partial y} = \frac{\nu}{\Pr}\left(1 + \frac{4}{3R}\right)\frac{\partial^2 T}{\partial y^2} + \frac{Q}{\rho C_p}\left(T - T_\infty\right) \tag{12}$$

Where $\Pr = \dfrac{\rho \nu C_p}{\kappa}$ and $R = \dfrac{\kappa k^*}{4\sigma_o T_\infty^3}$. We now define the similarity variables as

$$u = u_o U(\eta),\ w = u_o W(\eta),\ \theta(\eta) = \frac{\left(T - T_\infty\right)}{\left(T_w - T_\infty\right)},\ \varphi(\eta) = \frac{\left(C - C_\infty\right)}{\left(C_w - C_\infty\right)},\ \eta = \frac{y}{h} \tag{13}$$

Where $h\left(= h(t)\right)$ is a similarly parameter length scale and u_0 is the free stream velocity. In terms of $h(t)$, a convenient solution of (4) can be given by

$$v = -v_o\left(\frac{u}{h}\right) \tag{14}$$

Where v_0 is a non-dimensional transpiration parameter, clearly $v_0 > 0$ and $v_0 < 0$ indicates suction or injection respectively. Substituting equations (13) and (14) into equations (5), (6), (8) and (12) yields,

$$-\frac{h}{\nu}\frac{dh}{dt}\eta U' - v_o U' = \left(\frac{1}{1+\lambda}\right)U'' + (Gr)\theta(\cos\alpha) + (Gc)\varphi(\cos\alpha) + \frac{M}{\left(1+m^2\right)}(U+mW) \tag{15}$$

$$-\frac{h}{\nu}\frac{dh}{dt}\eta W' - v_o W' = W'' + \frac{M}{\left(1+m^2\right)}(mU - W) \tag{16}$$

$$-\frac{h}{\nu}\frac{dh}{dt}\eta\theta' - v_o\theta' = \frac{1}{\Pr}\left(1+\frac{4}{3R}\right)\theta'' + S\theta \tag{17}$$

$$-\frac{h}{\nu}\frac{dh}{dt}\eta\varphi' - v_o\varphi' = \frac{1}{Sc}\varphi'' - k_r\varphi \tag{18}$$

where, $Gr = g\beta h^2\frac{(T_w - T_\infty)}{\nu u_o}$, $Gc = g\beta^* h^2\frac{(C_w - C_\infty)}{\nu u_o}$, $M = \frac{\sigma\mu_e^2 B_o^2 h^2}{\nu\rho}$, $Sc = \frac{\nu}{D}$, $k_r = \frac{h^2 K_r}{\nu^2}$, $S = \frac{Qh^2}{\rho\nu C_p}$

Equations (15), (16), (17) and (18) are similar except for the term $\left(\frac{h}{\nu}\right)\left(\frac{dh}{dt}\right)$ where t appears explicitly. Thus, the similar condition requires that $\left(\frac{h}{\nu}\right)\left(\frac{dh}{dt}\right)$ must be constant. Hence it is assumed that

$$\left(\frac{h}{\nu}\right)\left(\frac{dh}{dt}\right) = C_1 \tag{19}$$

where, C_1 is an arbitrary constant. At $C_1 = 2$ and by integrating Equation (19), one obtain $h = 2\sqrt{\nu t}$ which defines the well-established scaling parameter for unsteady boundary layer problems. Hence, the similarity equations are obtained as

$$\left(\frac{1}{1+\lambda}\right)\frac{d^2U}{d\eta^2} + 2(\eta + a_o)\frac{dU}{d\eta} + (Gr)\theta(\cos\alpha) + (Gc)\varphi(\cos\alpha) - \frac{M}{\left(1+m^2\right)}(U+mW) = 0 \tag{20}$$

$$\frac{d^2W}{d\eta^2} + 2\left(\eta + a_o\right)\frac{dW}{d\eta} + \frac{M}{\left(1+m^2\right)}\left(mU - W\right) = 0 \tag{21}$$

$$\left(1+\frac{4}{3R}\right)\frac{d^2\theta}{d\eta^2} + 2(\mathrm{Pr})\left(\eta + a_o\right)\frac{d\theta}{d\eta} + \left(S\right)(\mathrm{Pr})\theta = 0 \tag{22}$$

$$\frac{d^2\varphi}{d\eta^2} + 2\left(Sc\right)\left(\eta + a_o\right)\frac{d\varphi}{d\eta} - \left(k_r\right)(Sc)\varphi = 0 \tag{23}$$

where, $a_o = \frac{v_o}{2}$.

The boundary conditions corresponding to the equations (20), (21), (22) and (23) are

$$\left.\begin{array}{l} U = 0, \quad W = 0, \quad \theta = 1, \quad \varphi = 1 \quad at\ \eta = 0 \\ U \to 0, \quad W \to 0, \quad \theta \to 0, \quad \varphi \to 0 \quad as\ \eta \to \infty \end{array}\right\} \tag{24}$$

In nomenclature section, all the symbols are defined. Of special significance for this type of flow and heat and mass transfer situation are the skin-friction coefficient, the Nusselt number *Nu* and the Sherwood number *Sh*. The skin-friction coefficients in the $x-$direction and $z-$direction, the local Nusselt number and the local Sherwood number are, respectively given by

$$\left.\begin{array}{l} \tau_x = \mu\left.\frac{\partial u}{\partial y}\right|_{y=0} = \frac{\mu u_o}{h}U'(0) \Rightarrow C_x = \frac{2\tau_x}{\rho u_o^2} = 2\mathrm{Re}^{-1}U'(0) \\ \&\ \tau_z = \mu\left.\frac{\partial w}{\partial y}\right|_{y=0} = \frac{\mu u_o}{h}W'(0) \Rightarrow C_z = \frac{2\tau_z}{\rho u_o^2} = 2\mathrm{Re}^{-1}W'(0) \end{array}\right\} \tag{25}$$

$$q_w = -\kappa\left.\frac{\partial T}{\partial y}\right|_{y=0} - \frac{4\sigma}{3k^*}\left(\frac{\partial T^4}{\partial y}\right)_{y=0} = -\theta'(0)\left(T_w - T_\infty\right)\frac{\kappa}{h}\left(1+\frac{4}{3R}\right)$$

$$\Rightarrow \quad Nu = -\left(1+\frac{4}{3R}\right)\theta'(0) \tag{26}$$

$$m_w = -D\left.\frac{\partial C}{\partial y}\right|_{y=0} = -\varphi'(0)\left(C_w - C_\infty\right)\frac{D}{h}$$

$$Sh = -\frac{m_w}{\left(C_w - C_\infty\right)}\frac{D}{h} = -\varphi'(0) \tag{27}$$

where, $\mathrm{Re} = \dfrac{u_o h}{\nu}$ is the Reynold's number.

3. METHOD OF SOLUTION BY FINITE DIFFERENCE METHOD:

The non-linear momentum and energy equations given in equations (20), (21), (22) and (23) are solved under the appropriate initial and boundary conditions (24) by the implicit finite difference method. The transport equations (20), (21), (22) and (23) at the grid point (*i*, *j*) are expressed in difference form using Taylor's expansion. The momentum equations reads.

$$\left(\frac{1}{1+\lambda}\right)\left(\frac{U_{i+1}^{j} - 2U_i^j + U_{i-1}^{j}}{(\Delta y)^2}\right) + 2(\eta + a_o)\left(\frac{U_{i+1}^{j} - U_i^j}{\Delta y}\right)$$

$$+ (Gr)(\cos\alpha)\theta_i^j + (Gc)(\cos\alpha)\varphi_i^j - \frac{M}{1+m^2}\left(U_i^j + mW_i^j\right) = 0 \quad (28)$$

$$\left(\frac{W_{i+1}^{j} - 2W_i^j + W_{i-1}^{j}}{(\Delta y)^2}\right) + 2(\eta + a_o)\left(\frac{W_{i+1}^{j} - W_i^j}{\Delta y}\right) + \frac{M}{1+m^2}\left(mU_i^j - W_i^j\right) = 0 \quad (29)$$

$$\left(1 + \frac{4}{3R}\right)\left(\frac{\theta_{i+1}^{j} - 2\theta_i^j + \theta_{i-1}^{j}}{(\Delta y)^2}\right) + 2(\mathrm{Pr})(\eta + a_o)\left(\frac{\theta_{i+1}^{j} - \theta_i^j}{\Delta y}\right) + S(\mathrm{Pr})\theta_i^j = 0 \quad (30)$$

$$\left(\frac{\varphi_{i+1}^{j} - 2\varphi_i^j + \varphi_{i-1}^{j}}{(\Delta y)^2}\right) + 2(Sc)(\eta + a_o)\left(\frac{\varphi_{i+1}^{j} - \varphi_i^j}{\Delta y}\right) - (k_r)(Sc)\varphi_i^j = 0 \quad (31)$$

where the indices i and j refer to y and t respectively. The initial and boundary conditions (24) yield.

$$\left.\begin{aligned} &U_i^0 = 0, \quad W_i^0 = 0, \quad \theta_i^0 = 0, \quad \varphi_i^0 = 0 \ \ \textit{for all } i, \\ &U_i^j = 0, \quad W_i^j = 0, \quad \theta_i^j = 1, \quad \varphi_i^j = 1 \ \ \textit{at } i = 0 \\ &U_M^j \to 0, W_M^j \to 0, \theta_M^j \to 0, \varphi_M^j \to 0 \end{aligned}\right\} \quad (32)$$

Thus the values of *U*, *W*, θ and ϕ at grid point $\eta = 0$ are known; hence the temperature and concentration fields have been solved at time $\eta_{i+1} = \eta_i + \Delta\eta$ using the known values of the previous time $\eta = \eta_i$ for all $i = 1, 2, \ldots\ldots, N-1$. Then the velocity field is evaluated using the already known value of temperature

and concentration fields obtained at $\eta_{i+1} = \eta_i + \Delta\eta$. These processes are repeated till the required solution of U, W, θ and ϕ is gained at convergence criteria.

$$abs\left|(U,\ W,\ \theta,\ \varphi)_{exact} - (U,\ W,\ \theta,\ \varphi)_{numerical}\right| < 10^{-3} \tag{33}$$

4. VALIDATION OF CODE

In order to establish the accuracy of the present method of solution, we first deal with the special case of our problem and compare with literature results of Chamkha et al. [22] in tables 1, 2 and 3. Tables 1, 2 and 3 illustrate the computational values of $U'(0)$, $W'(0)$, $-\theta'(0)$ and $-\varphi'(0)$ for a special case of our model when pertinent parameters $\alpha = \lambda = 0$. The comparison shows that the present results by finite difference method were in excellent agreement with the solutions of Chamkha et al. [22].

Table 1.
Comparison between the present numerical results with the results of Chamkha et al. [22] for various values of *Gr*, Pr and *M* when $\lambda = 0$ and $\alpha = 0.0$ in Chamkha et al. [22]

Gr	*Pr*	*M*	*Present numerical results*			*Results of Chamkha et al. [22]*		
			$U'(0)$	$W'(0)$	$-\theta'(0)$	$f'(0)$	$G'(0)$	$-\theta'(0)$
0.0	0.3	5.0	0.56847142	0.06507254	0.43581772	0.568575	0.06508	0.436954
	1.0		0.56847142	0.06507254	0.83051224	0.568575	0.06508	0.830676
5.0	0.3	5.0	2.66754418	0.44621784	0.43581772	2.667677	0.446024	0.436954
	1.0		2.26941532	0.30019465	0.83051224	2.26936	0.300199	0.830676
1.0	0.73	1.0	1.25704215	0.05714286	0.69184423	1.257009	0.057871	0.691974
		10.0	0.74513954	0.12134005	0.69184423	0.745692	0.121217	0.691974

Table 2.
Comparison between the present numerical results with the results of Chamkha et al. [22] for various values of *Gc*, *Sc* and *m* when $\lambda = 0$ and $\alpha = 0.0$ in Chamkha et al. [22]

Gc	*Sc*	*m*	*Present numerical results*			*Results of Chamkha et al. [22]*		
			$U'(0)$	$W'(0)$	$-\theta'(0)$	$f'(0)$	$G'(0)$	$-\theta'(0)$
0.0	0.2	0.5	0.36465215	0.05501225	0.72456612	0.364526	0.055001	0.724584
	0.6		0.36465215	0.05501225	1.13319852	0.364526	0.055001	1.1331985
2.0	0.2	0.5	1.10398554	0.17129664	0.72458662	1.103997	0.171305	0.724584
	0.6		0.93832684	0.12129467	1.33186445	0.938351	0.121386	1.331985
2.0	0.62	0.2	0.90596675	0.05115573	1.35726015	0.906068	0.051156	1.357259
		0.6	0.94577621	0.13963048	1.35726015	0.945865	0.139741	1.357259

Table 3.
Comparison between the present numerical results with the results of Chamkha et al. [22] for various values of S (Q), R, v_o and k_r when $\lambda = 0$ and $\alpha = 0.0$ in Chamkha et al. [22]

v_o	$S(Q)$	R	k_r	*Present numerical results*	*Results of Chamkha et al. [22]*
				$-\varphi'(0)$	$-\varphi'(0)$
		1.0	1.0	1.35725756	1.357258
			2.0	1.58004701	1.580046
	0.2	5.0		1.35725756	1.357258
0.5		10.0		1.35725756	1.357258
	0.4			1.35725756	1.357258
	0.8		1.0	1.35725756	1.357258
	- 0.4	1.0		1.35725756	1.357258
0.0	0.2			1.16483532	1.164834
0.8				1.48014512	1.480146

where, Q is the heat generation or absorption parameter (adapted from Chamkha et al. [22]).

5. RESULTS AND DISCUSSIONS

The set of nonlinear ordinary differential Eqs. (20), (21), (22) and (23) with boundary conditions (24) have been solved by using finite difference method. The numerical results of primary and secondary velocities, temperature and concentration profiles are presented with the help of curves in Figures 2-28.

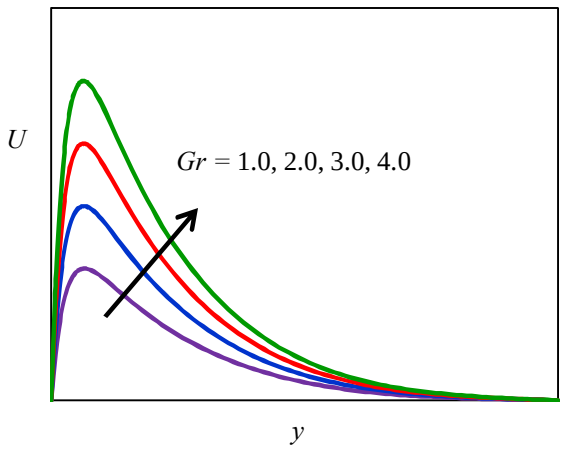

Figure 2: Effect of *Gr* on primary velocity profiles

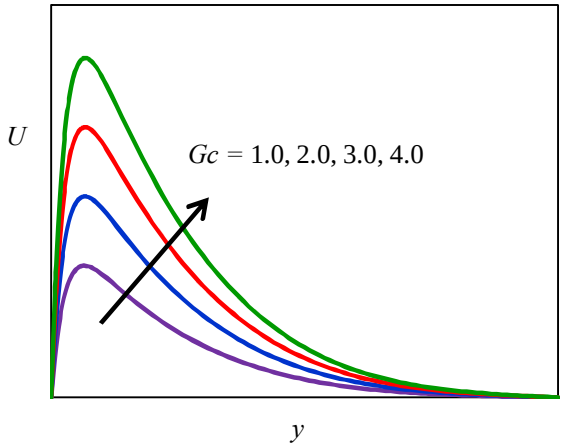

Figure 3: Effect of *Gc* on primary velocity profiles

For various values of Grashof number and Modified Grashof number, the velocity profiles *u* are plotted in Figs. 2 and 3. The Grashof number signifies the relative effect of the thermal buoyancy force to the viscous hydrodynamic force in the boundary layer. As expected, it is observed that there is a rise in the velocity due to the enhancement of thermal buoyancy force. Also, as *Gr* increases, the peak values of the velocity increases rapidly near the porous plate and then decays smoothly to the free stream velocity. The Modified Grashof number defines the ratio of the species buoyancy force to the viscous hydrodynamic force. As expected, the fluid velocity increases and the peak value is more distinctive due to increase in the species buoyancy force. The velocity distribution attains a distinctive maximum value in the vicinity of the plate and then decreases properly to approach the free stream value. It is noticed that the velocity increases with increasing values of Modified Grashof number.

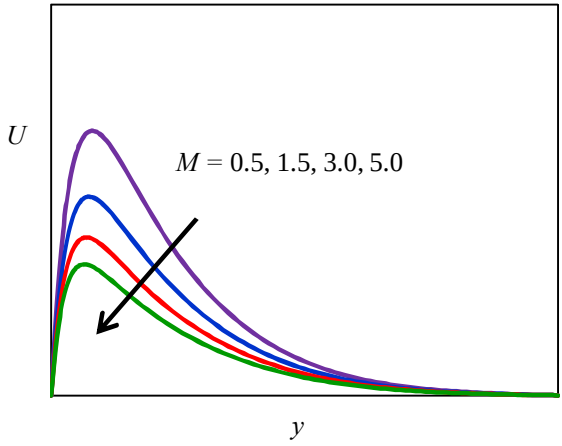

Figure 4: Effect of *M* on primary velocity profiles

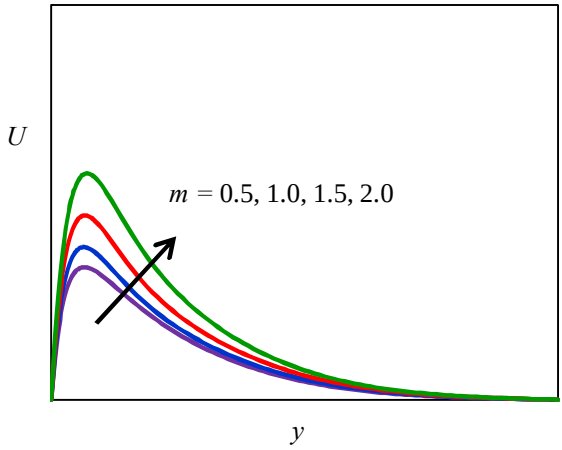

Figure 5: Effect of *m* on primary velocity profiles

The effects of magnetic field parameter on velocity distribution profiles across the boundary layer are presented in Figure 4. It is obvious that the effect of increasing values of the magnetic field parameter *M* results in a decreasing velocity distribution across the boundary layer. This is due to the fact that the effect of a transverse magnetic field give rise to a resistive type force called the Lorentz force. The force has the tendency to slow the motion of the fluid.

Figure 5 displays the effect of Hall current parameter *m* on the translational velocity distribution profiles. It is noticed that the Hall current parameter increases the velocity.

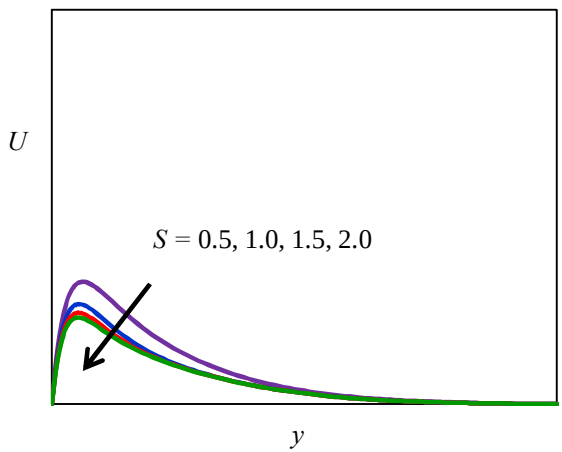

Figure 6: Effect of *S* on primary velocity profiles

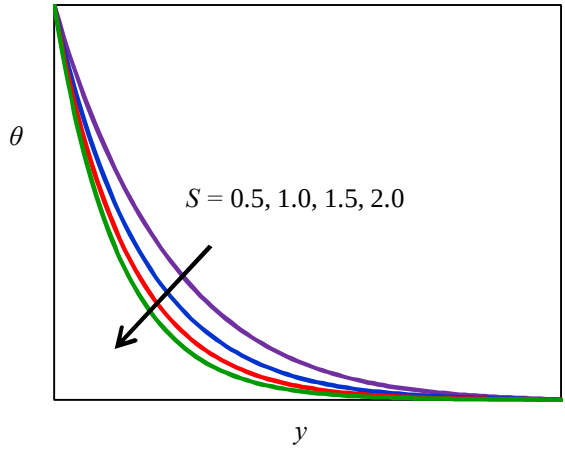

Figure 7: Effect of *S* on temperature profiles

Figures 6 and 7 illustrate the influence of heat source parameter on the primary velocity and temperature profiles respectively. Physically speaking, the presence of heat absorption (thermal sink) effects has the tendency to reduce the fluid temperature. This causes the thermal buoyancy effects to decrease resulting in a net reduction in the fluid velocity. These behaviours are clearly obvious from Figures 6 and 7 in which both the primary velocity and temperature distributions decrease as S increases. It is also observed that the both the hydrodynamic (velocity) and the thermal (temperature) boundary layers decrease as the heat absorption effects increase.

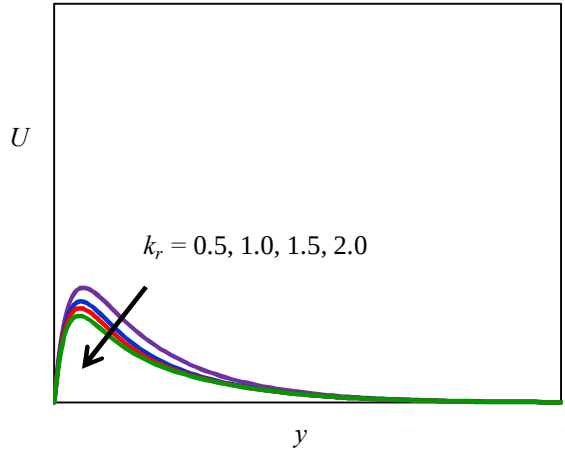

Figure 8: Effect of k_r on primary velocity profiles

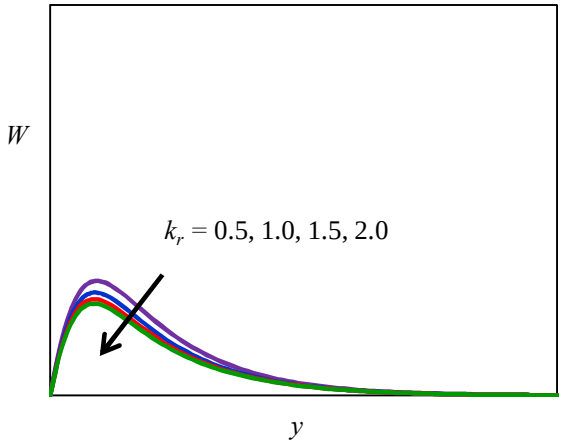

Figure 9. Effect of k_r on secondary velocity profiles

Figures 8 and 9 demonstrate the influence of chemical reaction parameter k_r on the primary fluid velocity (u) and secondary fluid velocity (w) respectively. As can be seen, an increase in the chemical reaction parameter (k_r) leads to an increase in the thickness of the velocity boundary layer; this shows that diffusion rate can be tremendously altered by chemical reaction (k_r). A temporal maximum of velocity profiles is clearly seen for increasing values of k_r. It should be mentioned here that physically positive values of k_r imply destructive reaction and negative values of k_r imply generative reaction. We studied the case of a destructive chemical reaction (k_r).

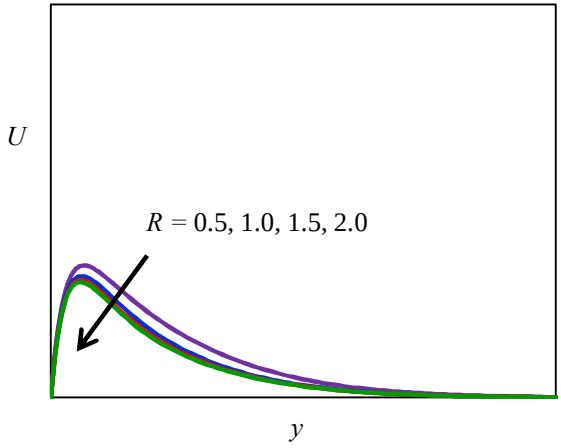

Figure 10: Effect of *R* on primary velocity profiles

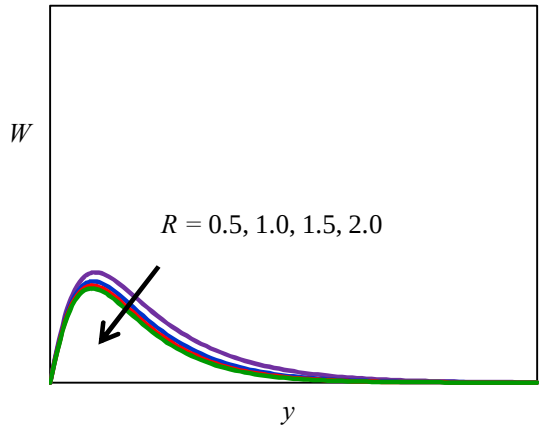

Figure 11: Effect of *R* on secondary velocity profiles

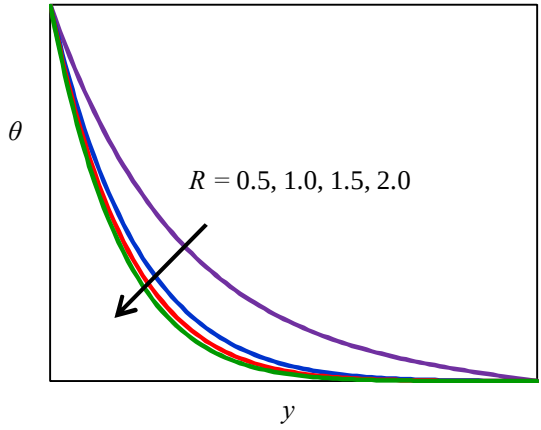

Figure 12: Effect of *R* on temperature profiles

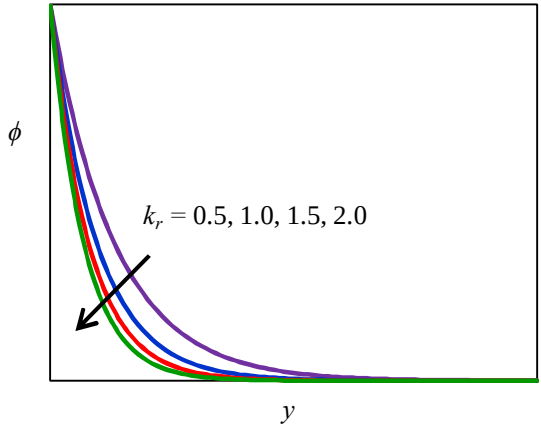

Figure 13: Effect of k_r on concentration profiles

Figs. 10, 11 and 12 illustrate the influence of thermal radiation on primary velocity, secondary fluid velocity and fluid temperature respectively. It is evident from these figures that, the thermal radiation leads to decrease in each of velocities and temperature. Physically, thermal radiation causes a fall in temperature of the fluid medium and thereby causes a fall in kinetic energy of the fluid particles. This results in a corresponding decrease in fluid velocities.

Fig. 13 shows the influence of a chemical reaction on concentration profiles. In this study, we are analyzing the effects of a destructive chemical reaction ($k_r > 0$). It is noticed that concentration distributions decrease when the chemical reaction increases. Physically, for a destructive case, chemical reaction takes place with many disturbances. This, in turn, causes high molecular motion, which results in an increase in the transport phenomenon, thereby reducing the concentration distributions in the fluid flow.

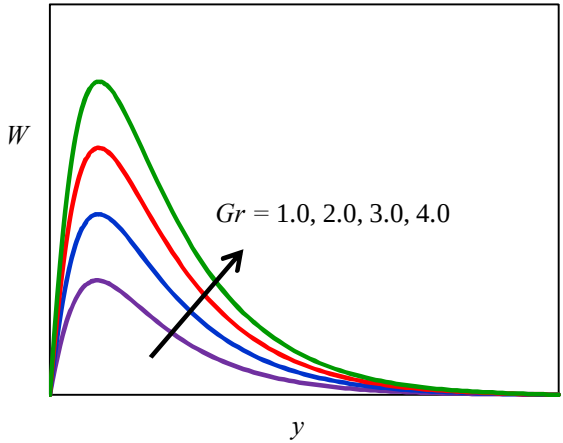

Figure 14: Effect of *Gr* on secondary velocity profiles

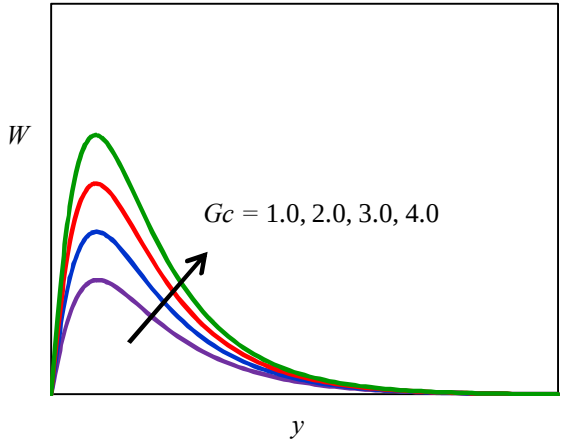

Figure 15: Effect of *Gc* on secondary velocity profiles

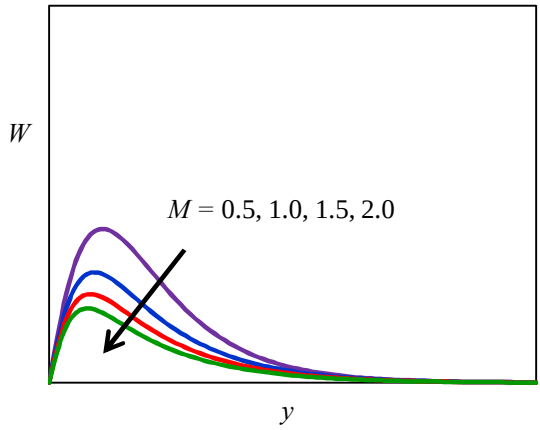

Figure 16: Effect of *M* on secondary velocity profiles

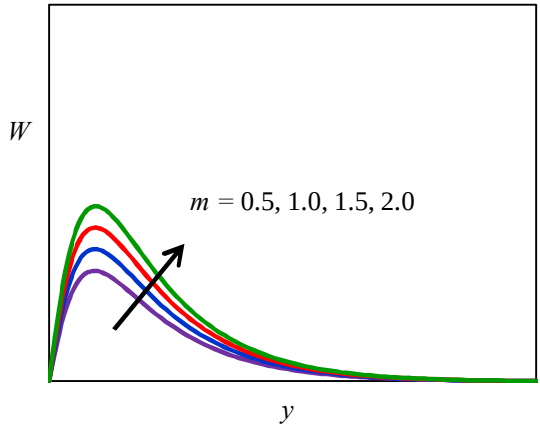

Figure 17: Effect of *m* on secondary velocity profiles

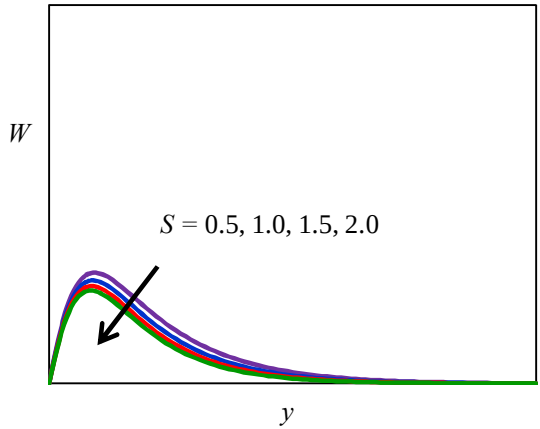

Figure 18: Effect of *S* on secondary velocity profiles

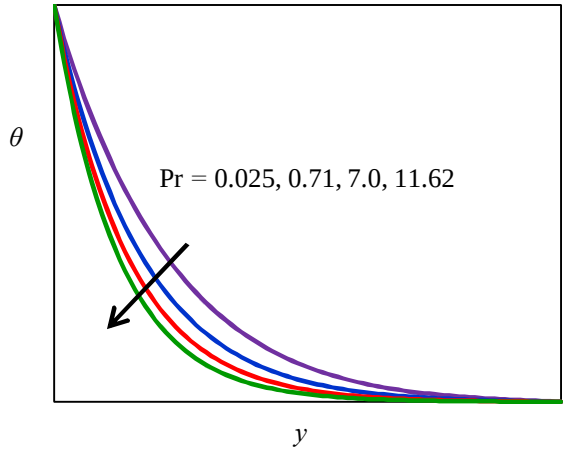

Figure 19: Effect of Pr on temperature profiles

In Figs. 14 and 15, we see the influence of the both heat and mass transfer on secondary velocity of the flow. It can be seen that as both the heat and mass transfer increases, this velocity component increases as well.

In Fig. 16, we have the influence of the Magnetic field parameter (Hartmann number) on the secondary velocity. It can be seen that as the values of this parameter increases, the secondary velocity increases.

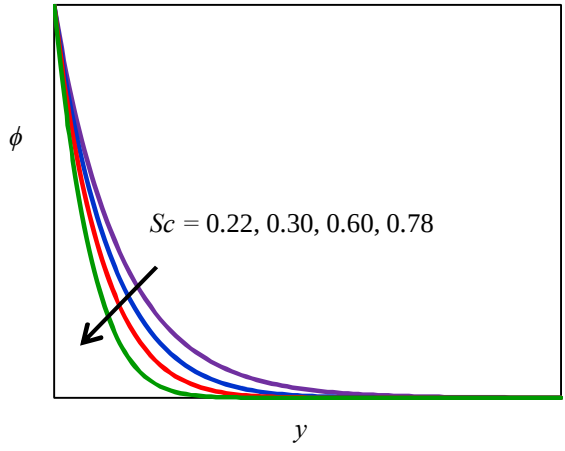

Figure 20: Effect of *Sc* on concentration profiles

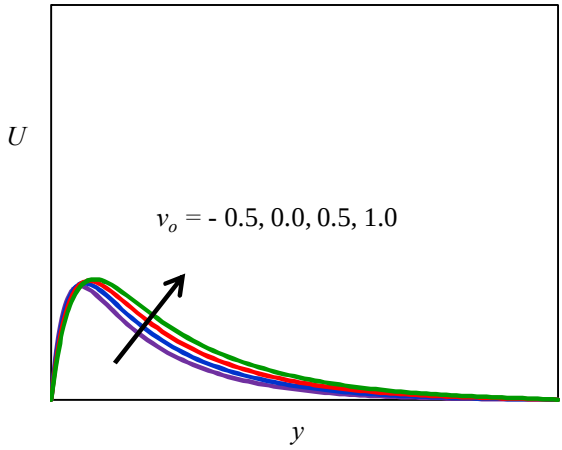

Figure 21: Effect of v_o on primary velocity profiles

In Fig. 17, we see that w profiles increase for $m < 1$ and decrease for $m > 1$. The effect of heat source parameter on the secondary velocity is as shown in the Fig. 18. From this figure the secondary velocity decreases with increasing values of S.

Fig. 19 presents the effect of the Prandtl number Pr on the temperature profiles. Increasing the value of Pr has the tendency to decrease the fluid temperature in the boundary layer as well as the thermal boundary layer thickness.

Fig. 20 shows the concentration field due to variation in Schmidt number for the gasses Hydrogen, Helium, Water-vapour and Ammonia. It is observed that concentration field is steadily for Hydrogen and falls rapidly for Water-vapour and Ammonia in comparison to Helium. Thus Hydrogen can be used for maintaining effective concentration field and Helium can be used for maintaining normal concentration field.

Figs. 21, 22, 23 and 24 depict the effect of suction/injection parameter v_o on primary, secondary velocities, temperature and concentration profiles against y keeping other parameters are constant. Suction/injection parameter is found to increase the primary, secondary velocities, temperature and concentration profiles at all points.

We discussed the effect of Jeffrey fluid parameter on both primary and secondary velocity profiles in Figs. 25 and 26 respectively. It is observed that Jeffrey fluid parameter increases the primary and secondary velocity profiles of flow field at all points.

The influence of angle of inclination parameter on both primary and secondary velocity profiles is as shown in the Figs. 27 and 28 respectively. From these figures, we observe that the velocities are decreasing with increasing values of angle of inclination parameter.

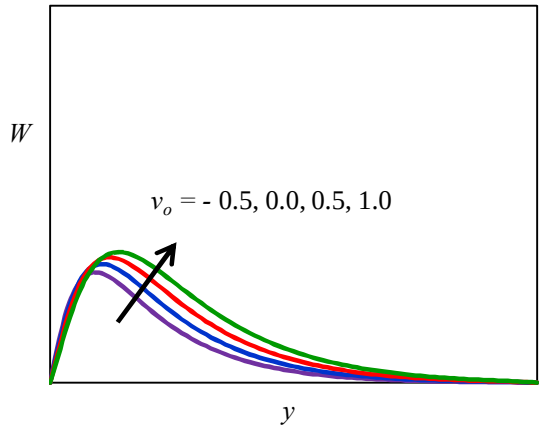

Figure 22: Effect of v_o on secondary velocity profiles

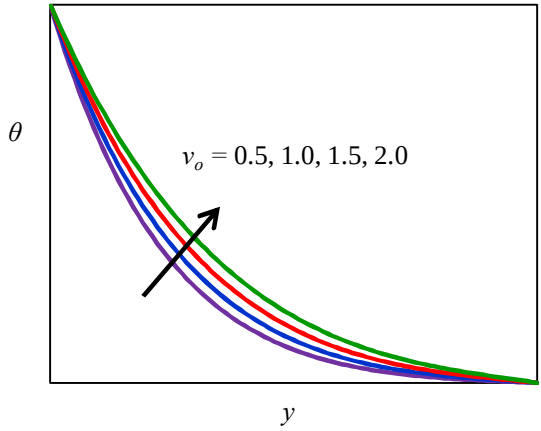

Figure 23: Effect of v_o on temperature profiles

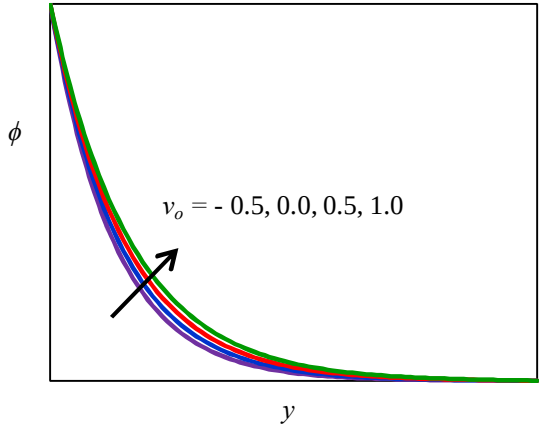

Figure 24: Effect of v_o on concentration profiles

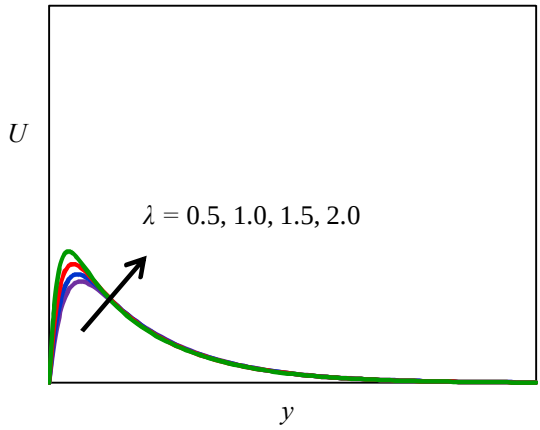

Figure 25: Effect of λ on primary velocity profiles

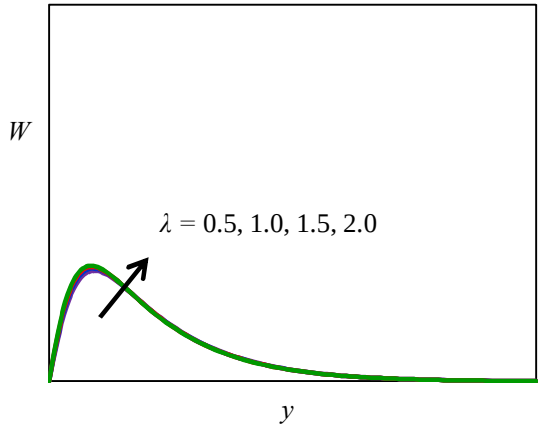

Figure 26: Effect of λ on secondary velocity profiles

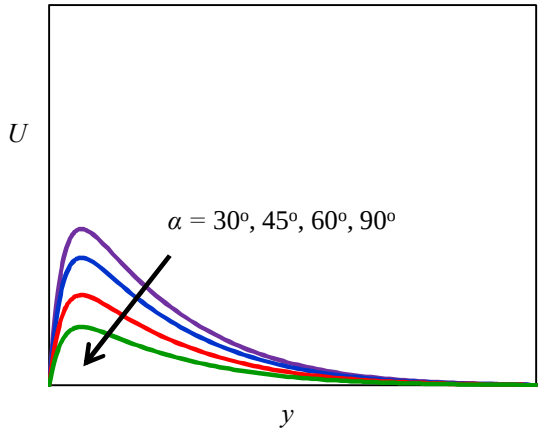

Figure 27: Effect of α on primary velocity profiles

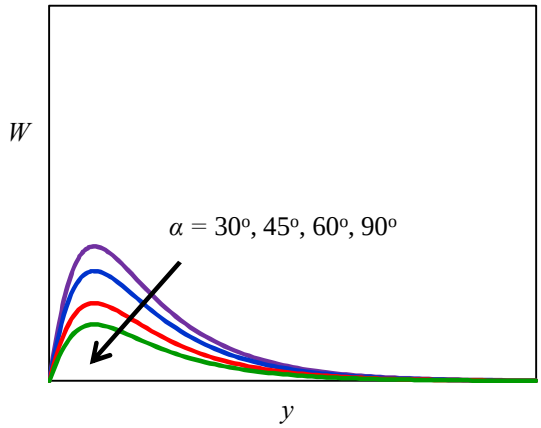

Figure 28: Effect of α on secondary velocity profiles

6. CONCLUSIONS:

We summarized below the following results of physical interest on the primary and secondary velocity profiles, temperature and the concentration profiles of the flow field and also on the wall shear stress and rate of heat transfer at the wall.

The Grashof number for heat and mass transfer has an accelerating effect on the flow velocities due to the enhancement in the buoyancy force.

Hall current tends to accelerate both primary and secondary fluid velocities throughout the boundary layer region.

Concentration buoyancy force tends to accelerate both the primary and secondary fluid velocities throughout the boundary layer region whereas mass diffusion has reverse effect on it throughout the boundary layer region.

In the presence of a uniform magnetic field, increase in the strength of the applied magnetic field decelerated the fluid motion along the wall of the plate inside the boundary layer.

The Prandtl number decreases the temperature of the flow field at all points

The effect of increasing Schmidt number is to reduce the concentration boundary layer thickness of the flow field at all points.

Primary and secondary fluid velocities are getting retarded with the progress of Jeffrey fluid parameter throughout the boundary layer region.

In order to ascertain the accuracy of the numerical results, the present results are compared with the existed results of Chamkha *et al*. [22] for skin friction coefficients due to primary and secondary velocity profiles, rate of heat and mass transfer. They are found to be in a good agreement.

References

[1] O. Anwar Bég, K. Abdel Malleque, M.N. Islam, Modelling of Ostwald-deWaele non-Newtonian flow over a rotating disk in a non-Darcian porous medium, Int J Appl Math Mech, 8 (2012), pp. 46–67

[2] S. Nadeem, Rashid Mehmood, Noreen Sher Akbar, Thermo-diffusion effects on MHD oblique stagnation point flow of a viscoelastic fluid over a convective surface Eur Phys J Plus, 129 (2014), p. 182 http://dx.doi.org/10.1140/epjp/i2014-14182-3.

[3] V.R. Prasad, B. Vasu, O. Anwar Bég, R. Parshad, Unsteady free convection heat and mass transfer in a Walters-B viscoelastic flow past a semi-infinite vertical plate: a numerical study, Therm Sci-Int Sci J, 15 (2) (2011), pp. 291–305.

[4] D. Tripathi, O. Anwar Bég, J. Curiel-Sosa, Homotopy semi-numerical simulation of peristaltic flow of generalized Oldroyd-B fluids with slip effects, Comput Methods Biomech Eng, 17 (4) (2014), pp. 433–442

[5] O. Anwar Bég, H.S. Takhar, R. Bharagava, V.R. Prasad, Numerical study of heat transfer of a third grade viscoelastic fluid in non-Darcian porous media with thermophysical effects, Phys Scr, 77 (2008), pp. 1–11.

[6] M.M. Rashidi, O. Anwar Bég, M.T. Rastegari, A study of non-Newtonian flow and heat transfer over a non-isothermal wedge using the homotopy analysis method, Chem Eng Commun, 199 (2012), pp. 231–256.

[7] R.R. Huilgol, Z. You, Application of the augmented Lagrangian method to steady pipe flows of Bingham, Casson and Herschel-Bulkley fluids, J Non-Newton Fluid Mech, 128 (2005), pp. 126–143

[8] V. Ramachandra Prasad, S. Abdul Gaffar, E. Keshava Reddy, O. Anwar Bég, Free convection flow and heat transfer of non-Newtonian tangent hyperbolic fluid from an isothermal sphere with partial slip, Arabian J Sci Eng, 39 (11) (2014), pp. 8157–8174.

[9] V. Ramachandra Prasad, S. Abdul Gaffar, E. Keshava Reddy, O. Anwar Bég, Computational study of non-Newtonian thermal convection from a vertical porous plate in a non-Darcy porous medium with Biot number effects, J Porous Media, 17 (2014), pp. 601–622.

[10] S. Nadeem, Rashid Mehmood, Noreen Sher Akbar, Non-orthogonal stagnation point flow of a nano non-Newtonian fluid towards a stretching surface with heat transfer, Int J Heat Mass Transf, 57 (2) (2013), pp. 679–689.

[11] G.K. Ramesh, B.J. Gireesha, Influence of heat source/sink on a Maxwell fluid over a stretching surface with convective boundary conditions in the presence of nanoparticles, Ain Shams Eng J, 5 (3) (2014), pp. 991–998.

[12] H. Jeffreys, The earth (4th ed.), Cambridge University Press, London (1929).

[13] R.B. Bird, R.C. Armstrong, O. Hassager, Dynamics of polymeric liquids, Fluid Dynam (2nd ed.), vol. 1, , Wiley (1987).

[14] J.R. Welty, C.E. Wicks, R.E. Wilson, Fundamentals of momentum, Heat and Mass Transfer (second ed.), Wiley (1976).

[15] M. Gnaneswara Reddy, Heat and mass transfer on magnetohydrodynamic peristaltic flow in a porous medium with partial slip, Alexandria Eng. J., 55 (2) (2016), pp. 1225–1234.

[16] R. Pfeffer, J. Happel, An analytical study of heat and mass transfer in nultiparticle systems at low Reynolds number, Am. Inst. Chem. Eng. J., 10 (1964), pp. 605–611.

[17] Atul Kumar Singh, Ajoy Kumar Singh, N.P. Singh, Heat and mass transfer in MHD flow of a viscous fluid past a vertical plate under oscillatory suction velocity, Indian J. Pure Appl. Math., 34 (3) (2003), pp. 429–442.

[18] A. Gul, I. Khan, S. Shafie, A. Khalid, A. Khan, Heat transfer in MHD mixed convection flow of a Ferrofluid along a vertical channel, PLoS ONE, 10 (11) (2015), p. e0141213.

[19] A. Gul, I. Khan, S. Shafie, Energy transfer in mixed convection MHD flow of nanofluid containing different shapes of nanoparticles in a channel filled with saturated porous medium, Nanoscale Res. Lett., 10 (2015), p. 490.

[20] N.A.M. Zin, I. Khan, S. Shafie, The impact silver nanoparticles on MHD free convection flow of Jeffrey fluid over an oscillating vertical plate embedded in a porous medium, J. Mol. Liq., 222 (2016), pp. 138–150.

[21] A. Khalid, I. Khan, S. Shafie, Heat transfer in ferrofluid with cylindrical shape nanoparticles past a vertical plate with ramped wall temperature embedded in a porous medium, J. Mol. Liq., 221 (2016), pp. 1175–1183.

[22] Ali Chamkha, M. A. Mansour and Abdelraheem Aly, Unsteady MHD free convective heat and mass transfer from a vertical porous plate with Hall current, thermal radiation and chemical reaction effects, Int. J. Numer. Meth. Fluids, Vol. 65, Issue 4, pp. 432–447 (2011).

[23] Sturdza P. An aerodynamic design method for supersonic natural laminar flow aircraft Ph. D. thesis. California, USA: Dept. Aeronautics and Astronautics, Stanford University; 2003.

[24] Chandrasekhar, S., (1961*). Hydrodynamic and Hydromagnetic Stability*, Oxford University Press: Oxford.

[25] Sparrow EM, Cess RD. Radiation Heat Transfer, Augment Edition. Hemisphere: Washington, DC, 1962.